The 21th Cambridge Workshop on Cool Stars, Stellar Systems, and the Sun
Edited by A. S. Brun, J. Bouvier, P. Petit

Solar neutrino fluxes show the signature of planet formation processes

Masanobu Kunitomo,[1] Tristan Guillot,[2] Gaël Buldgen[3]

[1] Department of Physics, Kurume University, 67 Asahimachi, Kurume, Fukuoka 830-0011, Japan
[2] Université Côte d'Azur, Observatoire de la Côte d'Azur, CNRS, Laboratoire Lagrange, Bd de l'Observatoire, CS 34229, 06304 Nice cedex 4, France
[3] Département d'Astronomie, Université de Genève, Chemin Pegasi 51, CH-1290 Versoix, Switzerland

Abstract

Solar evolutionary models are thus far unable to reproduce spectroscopic, helioseismic and neutrino constraints consistently, resulting in the so-called solar modeling problem. In parallel, planet formation models predict that the evolving composition of the protosolar disk, and thus, of the accreted gas by the proto-Sun must have been variable. In this talk, we show that solar evolutionary models including a realistic planet formation scenario lead to an increased core metallicity of up to 5%, implying that accurate neutrino flux measurements are sensitive to the initial stages of the formation of the Solar System. We demonstrate that in addition to macroscopic transport and increased opacities at the base of the convective envelope, the formation history of the Solar System constitutes a key element to resolve the current crisis of solar models.

1 Introduction

Stars are formed by accretion from a circumstellar disk where planets are formed. The accretion injects entropy and materials, which affect the thermal and chemical structures of stars. In a series of papers (Kunitomo *et al.*, 2017, 2018), we found that accretion can be crucial for some observational problems such as luminosity spreads in clusters (Hillenbrand, 2009) and chemical peculiarities in λ Boö stars (Murphy & Paunzen, 2017), solar twins (Meléndez *et al.*, 2009), and binary systems (Spina *et al.*, 2021). In this article, we focus on this process in the early Solar System (Kunitomo & Guillot, 2021; Kunitomo *et al.*, 2022).

There are two key features in the planet formation processes in the early Solar System. First, many solids were used for the planet formation processes. We estimated that the total amount of the solids is $\sim$150 $M_\oplus$, mainly in Jupiter, Saturn, and ejected materials from the outer Solar System (Kunitomo *et al.*, 2018). This is small compared to the total heavy element mass in the Sun, $\sim$5000 $M_\oplus$, but still, the planet formation processes can be important for the solar chemical structure as discussed below.

The other key feature is time variability. Planets are formed by the coagulation of dust grains (Kobayashi & Tanaka, 2021). They are initially μm-sized. Once they become cm-sized, which are called "pebbles", they rapidly fall onto the proto-Sun due to the frictional force with the disk gas (Adachi *et al.*, 1976). This leads to the evolution of the metallicity of accreted materials, $Z_{\rm accretion}$ (see Fig. 1 of Kunitomo & Guillot, 2021): The pebble drift results in the increase of $Z_{\rm accretion}$, and then, once pebbles deplete in the disk or a large protoplanet is formed, the accretion becomes metal-poor (Guillot *et al.*, 2014). Therefore, the variable composition of the accreted gas is naturally expected and in this article, we discuss how this affects the chemical structure of the Sun.

2 Method

We simulated the solar evolution from the protostellar phase to the present day. We use the one-dimensional stellar evolution code MESA (Modules for Experiments in Stellar Astrophysics) version 12115 (Paxton *et al.*, 2011, 2013, 2015, 2018, 2019). We refer the reader to the Paxton et al. papers and ours (Kunitomo *et al.*, 2017, 2018, 2022; Kunitomo & Guillot, 2021) for the full details of the computational method.

The solution at the present day is compared with constraints by spectroscopic and helioseismic observations. We iteratively optimized the solution using the simplex method (Nelder & Mead, 1965). We used six constraints: luminosity, effective temperature, surface metallicity, surface helium abundance, sound speed profile, and thickness of the surface convective zone (see Table 3 of Kunitomo & Guillot, 2021). Input parameters include the mixing-length parameter, overshooting parameter, initial composition, and parameters related to the planet formation processes. The reduced χ^2 value, indicating how well the observational constraints are reproduced, decreases by adjusting the input parameters. We performed this kind of simulation under a variety of settings.

The solar surface composition is still under debate (see, e.g., Asplund *et al.*, 2021; Magg *et al.*, 2022; Buldgen *et al.*, 2023). In this study, we adopted the commonly-used low-metallicity (Z) composition in Asplund *et al.* (2009, hereafter AGSS09). For reference, we also used the high-Z composition in Grevesse & Sauval (1998, hereafter GS98).

We note that we used six constraints (similar to Ayukov & Baturin, 2017) whereas many standard solar models (SSMs; solar models constructed with standard input physics) adopted only three (luminosity, effective temperature, and surface metallicity; see, e.g., Christensen-Dalsgaard *et al.*, 1996). The solutions depend on the number of constraints and thus we stress that the optimization procedure matters (see Sect. 3.3 of Kunitomo & Guillot, 2021).

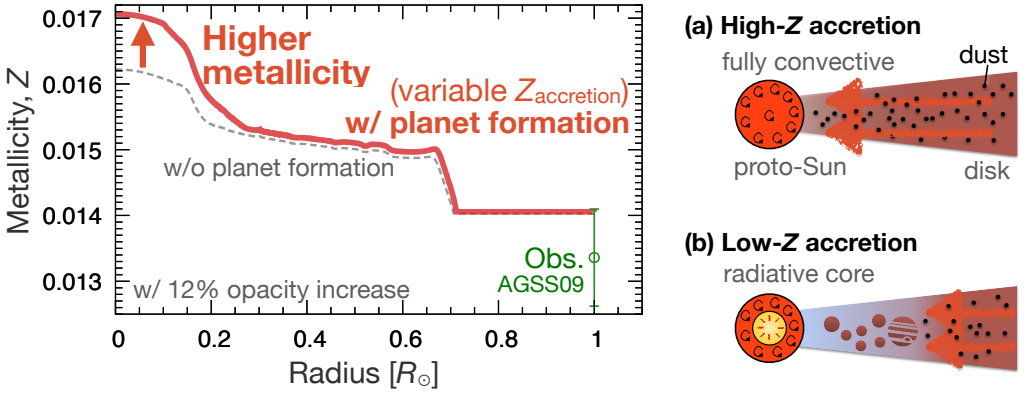

Figure 1: *Left panel*: metallicity profile in the interior of present-day Sun. The red solid and gray dashed lines indicate the models with and without planet formation processes (i.e., time-dependent and constant $Z_{\rm accretion}$, respectively). The former has a higher central metallicity but both models have a low surface metallicity that matches the observational constraint by AGSS09 (green circle with 1σ interval). See "K2-MZvar-A2-12" and "K2-A2-12" models in Table A.1 of Kunitomo & Guillot (2021) for details. *Right panel*: a schematic illustration of the protosolar accretion phase. In the early phase (panel (a)), the internal metallicity of the fully-convective proto-Sun homogeneously increases with time due to the high-Z accretion (i.e., dust drift; see text). Once protoplanets are formed or dust grains in the protosolar disk are exhausted (panel (b)), the disk metallicity decreases, and consequently, the solar surface metallicity decreases. However, the radiative core is detached from accretion and remains metal-rich. The signature of this variable $Z_{\rm accretion}$ remains in the solar core until the solar age as illustrated in the left panel.

3 Chemical structure of the present-day Sun

Figure 1 shows the metallicity profile of the present-day Sun in the models with and without planet formation processes (i.e., constant and time-dependent $Z_{\rm accretion}$, respectively). One finds that the evolving $Z_{\rm accretion}$ enhances the central metallicity by $\sim$5% and that the larger compositional gradient exists in the central region ($\lesssim$0.2 $R_\odot$). This result indicates that the solar core retains a clear signature of planet formation processes.

Here we discuss how accretion increases central metallicity. First, in the early phase ($<$1.7 Myr), accretion is metal-rich due to the pebble drift. The proto-Sun has a fully convective structure in this phase and thus the high-Z accreted materials are mixed in the entire region (i.e., the central metallicity increases).

Next, in the late accretion phase (2–10 Myr), the proto-Sun shrinks due to the Kelvin-Helmholtz contraction leading to the increasing internal temperature and the development of a radiative core. The low-Z accretion in this phase (see Sect. 1; the last 4% of the young Sun's mass in our best model) decreases the metallicity in the surface convective envelope (i.e., the surface metallicity decreases). On the other hand, the central radiative region is detached from accretion and thus the high central metallicity made in the early phase is preserved. This compositional gradient as an accretion signature remains until the solar age.

We stress that this accretion signature is closely related to both the planet formation processes and the thermal structure of the proto-Sun.

4 Implications for the solar abundance problem

In the last two decades, SSMs do not reproduce helioseismic and neutrino observations (so-called solar abundance problem or solar modeling problem; see, e.g., Montalban *et al.*, 2006; Vinyoles *et al.*, 2017; Buldgen *et al.*, 2019). Here, we discuss the implications of the compositional gradient of the present-day Sun due to the planet formation processes (Fig. 1) on the sound speed profile and neutrino fluxes.

4.1 Sound speed anomaly

The sound speed profile in the solar interior constrained by helioseismic observations (Basu *et al.*, 2009) is compatible with the SSMs with the old high-Z GS98 abundances. However, the SSMs with the new low-Z AGSS09 abundances poorly fit the constraints, especially around the base of the convective zone (BCZ). The gray and black lines in Fig. 2 show our non-accreting models with the GS98 and AGSS09 abundances, respectively (see models "noacc-GS98" and "noacc" in Kunitomo & Guillot, 2021).

Figure 2 shows that the sound-speed profile of the model with planet formation processes is almost identical to that of the non-accreting model with AGSS09, indicating that the variable $Z_{\rm accretion}$ cannot be the solution of the sound speed anomaly. This is because the accretion signature remains only in the central region ($\lesssim$0.2 $R_\odot$) and has no significant impact around the BCZ (see also Serenelli *et al.*, 2011).

Instead, we consider opacity increase in the solar interior, on which many theoretical (e.g., Christensen-Dalsgaard *et al.*, 2009; Serenelli *et al.*, 2009; Villante, 2010) and experimental (Bailey *et al.*, 2015) studies have focused. Figure 2 shows that, with a 12% opacity increase, the quality of the fit to the observational constraints is improved significantly and is even better than the non-accreting model using the GS98 abundances. The other spectroscopic and helioseismic observations are also well reproduced ($\chi^2 \lesssim 0.5$). We obtain the best results for a 12%–18% opacity increase (see Sect. 4.4 of Kunitomo & Guillot, 2021).

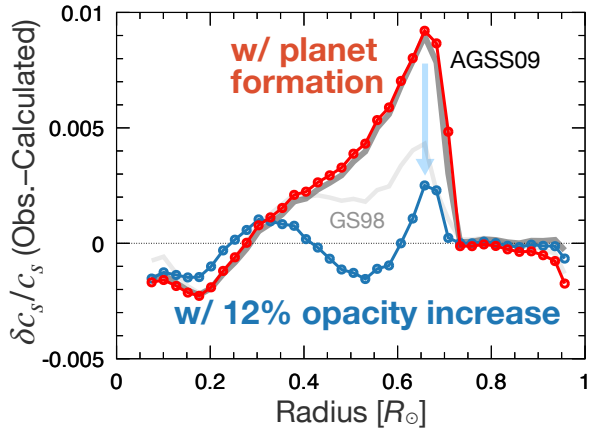

Figure 2: Radial profiles of observed minus calculated sound speed ($(c_{s,\mathrm{obs}} - c_{s,\mathrm{calc}})/c_{s,\mathrm{obs}}$). The gray and black lines show the results of non-accreting models with GS98 and AGSS09 compositions, respectively (see models "noacc-GS98" and "noacc" in Kunitomo & Guillot, 2021). The red and blue solid lines with circles show the non-standard models with the AGSS09 composition: the former includes the variable $Z_{\mathrm{accretion}}$ (i.e., planet formation processes) and the latter includes a 12% opacity increase (see models "MZvar" and "K2-A2-12" in Kunitomo & Guillot, 2021).

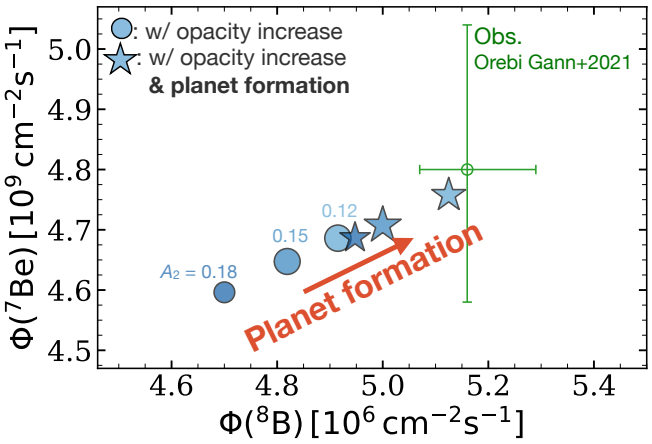

Figure 3: Neutrino fluxes obtained for the models with an opacity increase and planet formation. Shown are the models with an opacity increase (circles) and with both an opacity increase and a variable $Z_{\mathrm{accretion}}$ (star symbols). See "K2" and "K2-MZvar" models in Table A.1 of Kunitomo *et al.* (2022) for details. The colors show the opacity increase (12%, 15%, and 18%). The opacity increase in this range leads to a better match with spectroscopic and helioseismic observations ($\chi^2 \lesssim 0.5$). A higher opacity increase leads to lower $\Phi(^8\mathrm{B})$ and $\Phi(^7\mathrm{Be})$ values, whereas the planet formation processes lead to higher values. Our best model with both a 12% opacity increase and planet formation processes reproduces not only the observed constraints of neutrino fluxes (green circles with error bars; Orebi Gann *et al.*, 2021) but also the spectroscopic and helioseismic observations.

4.2 Metal-rich solar core compatible with observed neutrino fluxes

Recently, much effort has been made in the world for the measurement of solar neutrinos both from the proton-proton (*pp*) chain and the carbon-nitrogen-oxygen (CNO) cycle (Agostini *et al.*, 2018; Borexino Collaboration *et al.*, 2020; Orebi Gann *et al.*, 2021; Appel *et al.*, 2022). Solar neutrinos are important because they provide direct access to the solar core: the neutrino fluxes provide information about the temperature, temperature gradient, and composition in the core (Haxton & Serenelli, 2008; Gough, 2019). Similar to the sound speed, the high-Z GS98 SSMs better match the observed fluxes and no solar model that uses more recent AGSS09 abundances has reproduced both neutrino observations and other constraints simultaneously (see, e.g., Bahcall *et al.*, 2006; Vinyoles *et al.*, 2017).

Figure 3 shows the fluxes of $\Phi(^7\mathrm{Be})$ and $\Phi(^8\mathrm{B})$ neutrinos of the models with an opacity increase (model "K2"; circles) and with both an opacity increase and a variable $Z_{\mathrm{accretion}}$ (model "K2-MZvar"; star symbols). The K2 models indicate that a larger opacity increase leads to a lower internal metallicity and thus lower neutrino fluxes. The lower metallicity in the central region results in lower opacity and therefore lower central temperature. Since neutrino fluxes (i.e., nuclear reaction rates) depend on both composition and temperature (Bahcall & Ulmer, 1996), central metallicity is critical to determine the neutrino fluxes. The K2 models with a 12%–18% opacity increase match spectroscopic and helioseismic observations but the neutrino fluxes are not reproduced.

The models with a 12%–18% opacity increase and a variable $Z_{\mathrm{accretion}}$ have a low χ^2 ($\lesssim$0.5) value and higher neutrino fluxes because planet formation processes lead to a higher metallicity in the central region (Fig. 1). The higher central metallicity by up to 5% increases $\Phi(^7\mathrm{Be})$, $\Phi(^8\mathrm{B})$, and $\Phi(\mathrm{CNO})$ and lowers $\Phi(pp)$ and $\Phi(pep)$. In addition to a good fit to the $\Phi(^7\mathrm{Be})$ and $\Phi(^8\mathrm{B})$ constraints shown in Fig. 3, our best model (with a 12% opacity increase; see "K2-MZvar-A2-12" model in Table A.1 of Kunitomo *et al.*, 2022) reproduces the other fluxes as well within 1.3σ. Therefore, our models with planet formation processes fit all the helioseismic, spectroscopic, and neutrino constraints.

5 Future prospects

We simulated the formation and evolution of the Sun focusing on the effect of planet formation processes on the solar structure. We found that opacity increase is needed to reproduce helioseismic constraints but decreases neutrino fluxes. On the other hand, planet formation processes can increase the central metallicity by up to 5% and affect neutrino fluxes. Models including both planet formation processes and opacity increase reproduce all the observational constraints (i.e., spectroscopic, helioseismic, and neutrino).

More accurate neutrino fluxes measurements may lead to constraining the planet formation processes in the early Solar System (see Fig. A.4d of Kunitomo *et al.*, 2022) and are thus highly desirable (Orebi Gann *et al.*, 2021). We adopted a simplified model of $Z_{\mathrm{accretion}}$ but a realistic $Z_{\mathrm{accretion}}$ model in the early Solar System that matches the observations of Solar-System bodies is crucially important (see, e.g., Kruijer *et al.*, 2017; Kobayashi & Tanaka, 2021; Guillot *et al.*, 2022). Other input physics that affect neutrino fluxes (e.g., rotational mixing and solar wind mass loss; Eggenberger *et al.*,

2022; Zhang *et al.*, 2019) should also be constrained. The observed surface lithium abundance and rotation profiles are also key to constructing realistic solar models (Eggenberger *et al.*, 2022).

Acknowledgments

This work was supported by the JSPS KAKENHI (grant no. 20K14542). Numerical computations were carried out on PC cluster at the Center for Computational Astrophysics, National Astronomical Observatory of Japan. T.G. acknowledges funding from the Programme National de Planétologie. G.B. acknowledges funding from the SNF AMBIZIONE grant no. 185805 (Seismic inversions and modelling of transport processes in stars).

References

Adachi, I., Hayashi, C., & Nakazawa, K. 1976, Progress of Theoretical Physics, 56, 1756.
Agostini, M., Altenmüller, K., Appel, S., Atroshchenko, V., Bagdasarian, Z., *et al.* 2018, Nature, 562, 505.
Appel, S., Bagdasarian, Z., Basilico, D., Bellini, G., Benziger, J., *et al.* 2022, Phys. Rev. Lett., 129, 252701.
Asplund, M., Amarsi, A. M., & Grevesse, N. 2021, A&A, 653, A141.
Asplund, M., Grevesse, N., Sauval, A. J., & Scott, P. 2009, ARA&A, 47, 481.
Ayukov, S. V. & Baturin, V. A. 2017, Astronomy Reports, 61, 901.
Bahcall, J. N., Serenelli, A. M., & Basu, S. 2006, ApJS, 165, 400.
Bahcall, J. N. & Ulmer, A. 1996, Phys. Rev. D., 53, 4202.
Bailey, J. E., Nagayama, T., Loisel, G. P., Rochau, G. A., Blancard, C., *et al.* 2015, Nature, 517, 56.
Basu, S., Chaplin, W. J., Elsworth, Y., New, R., & Serenelli, A. M. 2009, ApJ, 699, 1403.
Borexino Collaboration, M., Agostini, Altenmüller, K., Appel, S., Atroshchenko, V., Bagdasarian, Z., *et al.* 2020, Nature, 587, 577.
Buldgen, G., Eggenberger, P., Noels, A., Scuflaire, R., Amarsi, A. M., *et al.* 2023, A&A, 669, L9.
Buldgen, G., Salmon, S. J. A. J., Noels, A., Scuflaire, R., Montalban, J., *et al.* 2019, A&A, 621, A33.
Christensen-Dalsgaard, J., Dappen, W., Ajukov, S. V., Anderson, E. R., Antia, H. M., *et al.* 1996, Science, 272, 1286.
Christensen-Dalsgaard, J., di Mauro, M. P., Houdek, G., & Pijpers, F. 2009, A&A, 494, 205.
Eggenberger, P., Buldgen, G., Salmon, S. J. A. J., Noels, A., Grevesse, N., *et al.* 2022, Nature Astronomy, 6, 788.
Gough, D. O. 2019, MNRAS, 485, L114.
Grevesse, N. & Sauval, A. J. 1998, SSRv, 85, 161.
Guillot, T., Fletcher, L. N., Helled, R., Ikoma, M., Line, M. R., *et al.* 2022, arXiv e-prints, arXiv:2205.04100.
Guillot, T., Ida, S., & Ormel, C. W. 2014, A&A, 572, A72.
Haxton, W. C. & Serenelli, A. M. 2008, ApJ, 687, 678.
Hillenbrand, L. A. 2009, In *IAU Symposium*, edited by E. E. Mamajek, D. R. Soderblom, & R. F. G. Wyse, *IAU Symposium*, vol. 258, pp. 81–94.
Kobayashi, H. & Tanaka, H. 2021, ApJ, 922, 16.
Kruijer, T. S., Burkhardt, C., Budde, G., & Kleine, T. 2017, Proceedings of the National Academy of Science, 114, 6712.
Kunitomo, M. & Guillot, T. 2021, A&A, 655, A51.
Kunitomo, M., Guillot, T., & Buldgen, G. 2022, A&A, 667, L2.
Kunitomo, M., Guillot, T., Ida, S., & Takeuchi, T. 2018, A&A, 618, A132.
Kunitomo, M., Guillot, T., Takeuchi, T., & Ida, S. 2017, A&A, 599, A49.
Magg, E., Bergemann, M., Serenelli, A., Bautista, M., Plez, B., *et al.* 2022, A&A, 661, A140.
Meléndez, J., Asplund, M., Gustafsson, B., & Yong, D. 2009, ApJL, 704, L66.
Montalban, J., Miglio, A., Theado, S., Noels, A., & Grevesse, N. 2006, Communications in Asteroseismology, 147, 80.
Murphy, S. J. & Paunzen, E. 2017, MNRAS, 466, 546.
Nelder, J. A. & Mead, R. 1965, The computer journal, 7, 308.
Orebi Gann, G. D., Zuber, K., Bemmerer, D., & Serenelli, A. 2021, Annual Review of Nuclear and Particle Science, 71, 491.
Paxton, B., Bildsten, L., Dotter, A., Herwig, F., Lesaffre, P., *et al.* 2011, ApJS, 192, 3.
Paxton, B., Cantiello, M., Arras, P., Bildsten, L., Brown, E. F., *et al.* 2013, ApJS, 208, 4.
Paxton, B., Marchant, P., Schwab, J., Bauer, E. B., Bildsten, L., *et al.* 2015, ApJS, 220, 15.
Paxton, B., Schwab, J., Bauer, E. B., Bildsten, L., Blinnikov, S., *et al.* 2018, ApJS, 234, 34.
Paxton, B., Smolec, R., Schwab, J., Gautschy, A., Bildsten, L., *et al.* 2019, ApJS, 243, 10.
Serenelli, A. M., Basu, S., Ferguson, J. W., & Asplund, M. 2009, ApJL, 705, L123.
Serenelli, A. M., Haxton, W. C., & Peña-Garay, C. 2011, ApJ, 743, 24.
Spina, L., Sharma, P., Meléndez, J., Bedell, M., Casey, A. R., *et al.* 2021, Nature Astronomy, 5, 1163.
Villante, F. L. 2010, ApJ, 724, 98.
Vinyoles, N., Serenelli, A. M., Villante, F. L., Basu, S., Bergström, J., *et al.* 2017, ApJ, 835, 202.
Zhang, Q.-S., Li, Y., & Christensen-Dalsgaard, J. 2019, ApJ, 881, 103.